Surface Wave Energy from Point Sources in Plane Layered Earth Models[1]

DAVID G. HARKRIDER[2] AND DON L. ANDERSON

Seismological Laboratory
California Institute of Technology, Pasadena

The total energy contained in a surface wave can be computed from its propagation-corrected spectrum by integrating over the surface of the earth and over the depth of the wave guide. The former requires knowledge of the radiation pattern of the source. The latter requires only a knowledge of the variation of physical properties with depth. In this paper the depth integration is performed for a continental and an oceanic earth model for three Rayleigh modes and four Love modes. The results are presented in tables and graphs in such a way that it is convenient to convert an observed surface wave displacement or displacement spectrum to total energy density. If the surface radiation pattern is known, the surface integration then yields the total energy in the observed spectrum. The partioning of energy between surface wave modes is computed for several simple sources at the surface and at depth, making it possible to estimate the energy contained in frequency bands or modes which are inaccessible for direct analysis. The increasing importance of the higher modes in the total energy budget at short periods and for channel depth sources is demonstrated. The shapes of the spectrums are diagnostic of source orientation and depth.

INTRODUCTION

Energy is an important concept in both theoretical and experimental seismology. It is involved in the derivation of the wave equation and in the variational methods of theoretical analysis. It has recently found application in the universal dispersion theory [*Anderson,* 1964], the earth anelasticity theory [*Anderson and Archambeau,* 1964], the inversion theory [*Archambeau and Anderson,* 1963], and the analytic calculation of group velocity [*Jeffreys,* 1961].

Energy radiation and energy partition of surface waves are important to our understanding of properties of the seismic source such as magnitude, mechanism, and depth. Even more fundamental is the question of energy balance of the earth. It has never been possible to measure all of the energy radiated in all directions at all frequencies from a single earthquake, much less the total annual tectonic energy release. It will never be possible, of course, to account for all the energy radiated by an earthquake, but the present methods of estimating energy from the magnitude are clearly unsatisfactory.

In this paper we compute the partition of energy among various surface wave modes for horizontal and vertical point sources at various depths in realistic earth models. Basic to this task is the excitation theory of *Harkrider* [1964].

In addition to explaining the presence or absence of individual modes and their relative energies, the theoretical results allow us to estimate the energy in frequency bands and modes that are not accessible for direct measurement. The partition functions and observed surface amplitudes can then be used in calculating the minimum seismic energy associated with an earthquake. Magnitudes and magnitude scales will have to be consistent with this observed minimum energy. Also, the strain energy release of a proposed source mechanism must be able to account for the observed seismic energy release.

In this paper we give expressions for the surface wave spectral energy density for various source depths and orientations and obtain the short- and long-period asymptotes. Relations are also given for obtaining the necessary medium response functions in terms of normalized energy integrals. These expressions are then

[1] Contribution 1386, Division of Geological Sciences, California Institute of Technology, Pasadena.

[2] Now at Brown University, Providence, Rhode Island.

evaluated and tabulated for a continental and an oceanic earth model.

The energy integrals given in this paper are useful in calculating a great variety of important seismic parameters, such as:

(*a*) Accurate values of the group velocity and the variation of relative excitation with frequency and mode.

(*b*) The effect of any parameter in any layer on the phase velocity [*Anderson,* 1964].

(*c*) The attenuation of surface waves, given the variation of anelasticity with depth [*Anderson and Archambeau,* 1964; *Anderson et al.,* 1965].

(*d*) The inverse of the two preceding problems.

(*e*) The energy for individual modes of surface waves from the observed or known spectrum of an identifiable mode.

(*f*) The energy partition as a function of depth of surface wave modes for seismic sources at the surface and at depth.

Symbols.

T^R, T^L, Rayleigh and Love kinetic energy density integrals, normalized to surface displacements.

V^R, V^L, Rayleigh and Love potential energy density integrals, normalized to surface displacements.

ω, angular frequency.

k_R, k_L, Rayleigh and Love angular wave numbers.

z, vertical or depth coordinate.

I_0^R, I_1^R, I_2^R, I_3^R, depth integrations defined by (3).

I_0^L, I_1^L, I_2^L, depth integrations defined by (4).

Q, W, normalized horizontal and vertical Rayleigh displacements.

V, normalized Love displacements.

$\dot{u}^*(z)/\dot{w}_0$, $\dot{v}(z)/\dot{v}_0$, $\dot{w}(z)/\dot{w}_0$, Haskell's plane wave particle velocity (or displacement) ratios at depth z.

$\sigma_R^*(z)$, Haskell's plane wave normal stress factor at depth z.

$\tau_R(z)$, $\tau_L^*(z)$, Haskell's Rayleigh and Love tangential stress factors at depth z.

d_j, thickness of layer j.

α_j, compressional velocity of layer j.

β_j, shear velocity of layer j.

ρ_j, density of layer j.

μ_j, rigidity of layer j.

λ_j, Lame's constant of layer j.

C_R, C_L, Rayleigh and Love phase velocities.

U_R, U_L, Rayleigh and Love group velocities.

A_R, A_L, Rayleigh and Love medium response functions.

μ_P, ρ_P, β_P, composite plate rigidity, density, and velocity defined by (14).

V_{Rj}, Rayleigh velocity of layer j.

γ_j, layer j coefficient defined by (16).

E^R, E^L, Rayleigh and Love spectrum energy densities per unit propagation path.

r, epicenter distance.

θ, azimuth angle.

h, source depth.

$[w_0(r, \theta, h)]_R$, vertical spectral surface displacement for Rayleigh waves.

$[v_0(r, \theta, h]_L$, horizontal spectral surface displacement for Love waves.

$\langle L \rangle$, spectral source strength.

E_V^R, E_V^L, Rayleigh and Love spectrum energy densities per unit propagation path for a vertical force.

E_H^R, E_H^L, Rayleigh and Love spectrum energy densities per unit propagation path for horizontal force.

Fundamental Formulas

The basic integrals for kinetic and potential energy density, normalized to the surface displacement, are given by

$$\begin{aligned} 2T^R &= \omega^2 I_0^R \\ 2V^R &= k_R^2 I_1^R + 2k_R I_2^R + I_3^R \end{aligned} \tag{1}$$

for Rayleigh waves and

$$\begin{aligned} 2T^L &= \omega^2 I_0^L \\ 2V^L &= k_L^2 I_1^L + I_2^L \end{aligned} \tag{2}$$

for Love waves, with

$$\begin{aligned} I_0^R &= \int_0^\infty \rho(Q^2 + W^2)\, dz \\ I_1^R &= \int_0^\infty \{(\lambda + 2\mu)Q^2 + \mu W^2\}\, dz \\ I_2^R &= \int_0^\infty \left\{\lambda Q \frac{dW}{dz} - \mu W \frac{dQ}{dz}\right\} dz \\ I_3^R &= \int_0^\infty \left\{(\lambda + 2\mu)\left(\frac{dW}{dz}\right)^2 + \mu\left(\frac{dQ}{dz}\right)^2\right\} dz \end{aligned} \tag{3}$$

and

$$I_0^L = \int_0^\infty \rho V^2 \, dz$$

$$I_1^L = \int_0^\infty \mu V^2 \, dz \qquad (4)$$

$$I_2^L = \int_0^\infty \mu \left(\frac{dV}{dz}\right)^2 dz$$

[*Jeffreys*, 1961]. The normalized displacements and displacement derivatives in the integrands of (3) and (4) can be expressed in terms of the Thomson-Haskell layer vector elements [*Haskell*, 1953]:

$$Q = \dot{u}^*(z)/\dot{w}_0$$

$$W = \dot{w}(z)/\dot{w}_0$$

$$\frac{dQ}{dz} = \frac{k_R}{\mu}\left\{\mu\left[\frac{\dot{w}(z)}{\dot{w}_0}\right] + \left[\frac{\tau_R(z)C_R}{\dot{w}_0}\right]\right\} \qquad (5)$$

$$\frac{dW}{dz} = -\frac{k_R}{(\lambda + 2\mu)} \cdot \left\{\lambda\left[\frac{\dot{u}^*(z)}{\dot{w}_0}\right] + \left[\frac{\sigma_R{}^*(z)C_R}{\dot{w}_0}\right]\right\}$$

and

$$V = \dot{v}(z)/\dot{v}_0$$

$$dV/dz = -(k_L/\mu)[\tau_L{}^*(z)C_L/\dot{v}_0] \qquad (6)$$

for a layered half-space composed of n elastic layers, where $\lambda_j = \rho_j(\alpha_j{}^2 - 2\beta_j{}^2)$ and $\mu_j = \rho_j\beta_j{}^2$. For computing purposes the relations between the vector elements, the phase velocities C_R and C_L, and the Thomson-Haskell layer matrices can be found in *Harkrider* [1964].

The Thomson-Haskell matrix technique has been used in two ways to evaluate the energy integrals. *Wu* [1966] used the matrix method in calculating values of the integrands at various depths for the fundamental modes and then computed the kinetic energy in integrals of (1) and (2) by numerical integration. *Anderson* [1964] used the matrix-calculated eigenfunctions in an analytic evaluation of the Love wave integrals. Anderson's technique is used in this paper.

The energy integrals can be used in calculating group velocity and the medium response without differentiation. Group velocity is determined by equating the kinetic and potential energy expressions in (1) and (2) and then invoking Rayleigh's principle [*Meissner*, 1926; *Jeffreys*, 1934, 1961]. The resulting expressions for group velocity are

$$U_R = (I_1{}^R + I_2{}^R/k_R)/(C_R I_0{}^R) \qquad (7)$$

$$U_L = I_1{}^L/(C_L I_0{}^L) \qquad (8)$$

This technique has been extended to group velocity calculations for spherical earth models by *Takeuchi et al.* [1962, 1964] and *Kovach and Anderson* [1964].

A modification of this technique allows one to calculate the changes in Rayleigh and Love wave phase velocities resulting from changes in the physical properties of the wave guide [*Jeffreys*, 1961; *Anderson*, 1964; *Takeuchi et al.*, 1964]. These perturbations can, in turn, be used for the calculation of the attenuation of surface waves as a function of period for realistic anelastic earth models [*Anderson and Archambeau*, 1964; *Anderson et al.*, 1965].

Integral relations similar to (7) and (8) can also be obtained for the medium response. Comparing the two-dimensional or line-source solutions of Neigaus [*Kellis-Borok and Yanovskaya*, 1962] with the three-dimensional or point-source solutions of *Harkrider* [1964], we see that the medium response can be expressed as

$$A_R = [2C_R U_R I_0{}^R]^{-1} = [2(I_1{}^R + I_2{}^R/k_R)]^{-1} \qquad (9)$$

$$A_L = [2C_L U_L I_0{}^L]^{-1} = [2I_1{}^L]^{-1} \qquad (10)$$

It is interesting that in (7), (8), (9), and (10) we are able to express the group velocity and the medium response in terms of the normalized energies which are used to calculate phase velocity perturbations [*Anderson*, 1964; *Takeuchi et al.*, 1964]. These relations make it convenient to calculate partial derivatives, not only for phase velocity but for the complete spectral response of any reasonable structure due to a change of elastic parameter at depth.

By using analytical expressions for the depth integrations, we were able to derive the short- and long-period limits for the fundamental mode Rayleigh and Love wave energy integrals. For high frequencies, the asymptotic form of $I_0{}^L$ is

$$I_0{}^L \rightarrow d_1\rho_1/2 \qquad (11)$$

TABLE 1. Layer parameters for the oceanic and shield earth models.

Ocean

D	ALPHA	BETA	RHO	MU	LAMDA	DEPTH	M
5.00	1.5200	0.	1.0300	0.	2.379712	2.50	0
1.00	2.1000	1.0000	2.1000	2.100000	5.061000	5.50	1
5.00	6.4100	3.7000	3.0660	41.973539	42.029035	8.50	2
9.00	8.1100	4.6060	3.4000	72.131800	79.361530	15.50	3
5.00	8.1200	4.6110	3.4000	72.288488	79.599974	22.50	4
15.00	8.1200	4.6100	3.4000	72.257137	79.662676	32.50	5
20.00	8.0100	4.5600	3.3700	70.074429	76.070675	50.00	6
20.00	7.9500	4.5600	3.3700	70.074429	72.843563	70.00	7
20.00	7.7100	4.4000	3.3700	65.243197	69.840218	90.00	8
20.00	7.6800	4.3400	3.3300	62.722546	70.966294	110.00	9
20.00	7.7770	4.3400	3.3300	62.722546	75.959060	130.00	10
20.00	7.8500	4.3400	3.3300	62.722546	79.757827	150.00	11
20.00	8.1000	4.4500	3.3300	65.942324	86.596643	170.00	12
20.00	8.1200	4.4500	3.3300	65.942324	87.676895	190.00	13
20.00	8.1200	4.4500	3.3300	65.942324	87.676895	210.00	14
20.00	8.1200	4.4500	3.3300	65.942324	87.676895	230.00	15
20.00	8.1200	4.4500	3.3300	65.942324	87.676895	250.00	16
20.00	8.1200	4.4500	3.3500	66.338373	88.203485	270.00	17
20.00	8.1200	4.4500	3.3600	66.536399	88.466776	290.00	18
20.00	8.1200	4.4500	3.3700	66.734424	88.730070	310.00	19
20.00	8.1200	4.4500	3.3800	66.932448	88.993366	330.00	20
20.00	8.2400	4.5000	3.3900	68.647499	92.877855	350.00	21
10.00	8.3000	4.5300	3.4400	70.591894	95.797806	365.00	22
20.00	8.3600	4.5600	3.5000	72.777597	99.058397	380.00	23
25.00	8.7500	4.7950	3.6840	84.702617	112.651014	402.50	24
20.00	9.1500	5.0400	3.8800	98.558205	127.726883	425.00	25
10.00	9.4300	5.2170	3.9000	106.146643	134.513813	440.00	26
20.00	9.7600	5.4000	3.9200	114.307198	144.795391	455.00	27
25.00	9.7650	5.4000	3.9330	114.686278	145.659540	477.50	28
25.00	9.7750	5.4000	3.9480	115.123677	146.986506	502.50	29
25.00	9.7800	5.4000	3.9600	115.471598	147.820463	527.50	30
25.00	9.7840	5.4000	3.9880	116.290077	149.177738	552.50	31
25.00	9.7880	5.4000	4.0220	117.281517	150.764442	577.50	32
25.00	9.7920	5.4000	4.0560	118.272958	152.356596	602.50	33
25.00	9.7960	5.4000	4.0900	119.264398	153.954199	627.50	34
25.00	9.8000	5.4000	4.1200	120.139196	155.406395	652.50	35
25.00	10.1630	5.6000	4.1650	130.614395	168.959763	677.50	36
25.00	10.4880	5.8000	4.2120	141.691675	179.928814	702.50	37
25.00	10.8180	6.1000	4.2570	158.402966	181.387039	727.50	38
25.00	11.1200	6.2000	4.3000	165.291996	201.129906	752.50	39
25.00	11.1350	6.2050	4.4750	172.296558	210.254181	777.50	40
25.00	11.1500	6.2100	4.6330	178.667469	218.651192	802.50	41
25.00	11.1650	6.2180	4.7970	185.468922	227.042854	827.50	42
25.00	11.1800	6.2300	4.9400	191.735720	233.991001	852.50	43
25.00	11.2240	6.2500	4.9425	193.066404	236.514317	877.50	44
25.00	11.2670	6.2750	4.9450	194.712463	238.319519	902.50	45
25.00	11.3100	6.2970	4.9475	196.179302	240.506287	927.50	46
25.00	11.3500	6.3220	4.9500	197.840031	241.991287	952.50	47
25.00	11.3920	6.3400	4.9517	199.036549	244.546944	977.50	48
25.00	11.4340	6.3600	4.9534	200.363043	246.863354	1002.50	49
25.00	11.4760	6.3750	4.9550	201.374296	249.817837	1027.50	50
25.00	11.5180	6.3900	4.9567	202.392466	252.792294	1052.50	51
25.00	11.5600	6.4050	4.9584	203.413521	255.781784	1077.50	52
25.00	11.6000	6.4210	4.9600	204.497028	258.423523	1102.50	53

Shield

D	ALPHA	BETA	RHO	MU	LAMDA	DEPTH	M
10.00	6.1000	3.5400	2.5500	31.955579	30.974339	5.00	1
6.50	6.1000	3.5400	2.5500	31.955579	30.974339	13.25	2
5.00	6.4000	3.7000	3.0800	42.165199	41.826400	19.00	3
5.00	6.7000	3.9200	3.4200	52.553087	48.417622	24.00	4
5.00	6.7000	3.9200	3.4200	52.553087	48.417622	29.00	5
3.50	6.7000	3.9200	3.4200	52.553087	48.417622	33.25	6
5.00	8.1500	4.7500	3.4200	77.163750	72.837444	37.50	7
20.00	8.1600	4.7500	3.4200	77.163750	73.395247	50.00	8
20.00	8.2100	4.7500	3.4200	77.163750	76.194515	70.00	9
20.00	8.2600	4.7500	3.4200	77.163750	79.010887	90.00	10
20.00	8.3200	4.7500	3.4200	77.163750	82.413103	110.00	11
20.00	8.3000	4.7000	3.4000	75.105998	84.013996	130.00	12
20.00	8.2840	4.5400	3.4000	71.319757	90.684305	150.00	13
20.00	8.2840	4.5400	3.4000	70.079437	93.164946	170.00	14
20.00	8.2840	4.5400	3.4100	70.285554	93.438961	190.00	15
20.00	8.2840	4.5400	3.4200	70.491670	93.712975	210.00	16
20.00	8.2840	4.5400	3.4500	71.110018	94.535019	230.00	17
20.00	8.2840	4.5400	3.4500	71.110018	94.535019	250.00	18
20.00	8.2840	4.5400	3.4500	71.110018	94.535019	270.00	19
20.00	8.2840	4.5400	3.4500	71.110018	94.535019	290.00	20
20.00	8.2840	4.5400	3.4500	71.110018	94.535019	310.00	21
20.00	8.2840	4.5400	3.4500	71.110018	94.535019	330.00	22
20.00	8.3130	4.5400	3.4500	71.110018	96.195551	350.00	23
10.00	8.5070	4.6430	3.4500	74.373197	100.926821	365.00	24
20.00	8.7000	4.7500	3.4500	77.840024	105.449245	380.00	25
25.00	8.7400	4.7500	3.6600	82.578750	114.421106	402.50	26
20.00	8.7600	4.7500	3.8800	87.542500	122.656883	425.00	27
10.00	9.0380	5.0000	3.9000	97.499999	123.573225	440.00	28
20.00	9.4890	5.2500	3.9200	108.044999	136.871187	455.00	29
25.00	9.5000	5.2530	3.9330	108.527235	137.898777	477.50	30
25.00	9.5160	5.2570	3.9480	109.107119	139.293953	502.50	31
25.00	9.5260	5.2600	3.9600	109.563694	140.221516	527.50	32
25.00	9.5760	5.2850	3.9880	111.389723	142.919250	552.50	33
25.00	9.6300	5.3130	4.0220	113.550887	145.922029	577.50	34
25.00	9.6830	5.3400	4.0560	115.659271	148.973991	602.50	35
25.00	9.7360	5.3670	4.0900	117.811175	152.067495	627.50	36
25.00	9.7820	5.3900	4.1200	119.694649	154.843288	652.50	37
25.00	10.0140	5.5180	4.1650	126.817265	164.032475	677.50	38
25.00	10.1800	5.6300	4.2120	133.507339	169.484978	702.50	39
25.00	10.1900	5.7460	4.2570	140.551306	160.927654	727.50	40
25.00	10.4920	5.8500	4.3000	147.156744	179.039375	752.50	41
25.00	10.6770	5.9500	4.4750	158.426184	193.290142	777.50	42
25.00	10.8520	6.0440	4.6330	169.243189	207.123043	802.50	43
25.00	11.0250	6.1400	4.7970	180.844978	221.388382	827.50	44
25.00	11.1800	6.2300	4.9400	191.735720	233.991001	852.50	45
25.00	11.2240	6.2500	4.9425	193.066404	236.514317	877.50	46
25.00	11.2670	6.2750	4.9450	194.712463	238.319519	902.50	47
25.00	11.3100	6.2970	4.9475	196.179302	240.506287	927.50	48
25.00	11.3500	6.3220	4.9500	197.840031	241.991287	952.50	49
25.00	11.3920	6.3400	4.9517	199.036549	244.546944	977.50	50
25.00	11.4340	6.3600	4.9534	200.363043	246.863354	1002.50	51
25.00	11.4760	6.3750	4.9550	201.374296	249.817837	1027.50	52
25.00	11.5180	6.3900	4.9567	202.392466	252.792294	1052.50	53
25.00	11.5600	6.4050	4.9584	203.413521	255.781784	1077.50	54
25.00	11.6000	6.4210	4.9600	204.497028	258.423523	1102.50	55

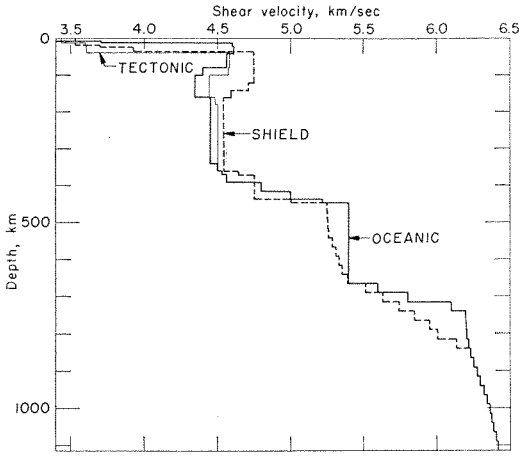

Fig. 1. Shear velocity as a function of depth for oceanic, tectonic, and shield earth models [*Anderson and Toksöz*, 1966; *Anderson* 1966].

and from (10)

$$A_L = (\mu_1 d_1)^{-1} \tag{12}$$

since $C_L \rightarrow U_L \rightarrow \beta_1$ as $\omega \rightarrow \infty$. For long periods of the fundamental Love mode, ${I_0}^L$ can be expressed in the limit as

$${I_0}^L \rightarrow {\mu_n}^2/[2\omega^2 d_p \mu_p({\beta_n}^2/{\beta_p}^2 - 1)] \tag{13}$$

where the subscript 1 designates the surface layer and n the nth layer or half-space. The new quantities are defined by

$$\mu_p = \sum_{j=1}^{n-1} \frac{\mu_j d_j}{d_p}$$

$$\rho_p = \sum_{j=1}^{n-1} \frac{\rho_j d_j}{d_p} \tag{14}$$

$$d_p = \sum_{j=1}^{n-1} d_j$$

and ${\beta_p}^2 = \mu_p/\rho_p$

From (10) we obtain the long-period limit

$$A_L = \omega^2 \, d_p \mu_p({\beta_n}^2/{\beta_p}^2 - 1)/(\beta_n \mu_n)^2 \tag{15}$$

using the limits

$$C_L \rightarrow U_L \rightarrow \beta_n \quad \text{as} \quad \omega \rightarrow 0$$

For Rayleigh waves the high-frequency and long-period asymptotes are

$${I_0}^R \rightarrow 2 V_{Ri} \rho_i D_i/\omega(1 - {V_{Ri}}^2/{\alpha_i}^2)^{1/2} \tag{16}$$

where

$$D_i = {\beta_i}^2 {\gamma_i}^2({\alpha_i}^2 + {\beta_i}^2 - 2{V_{Ri}}^2)/[\alpha_i V_{Ri}(\gamma_i - 1)]^2 - (\gamma_i - 1)$$

$$\gamma_i = 2(\beta_i/V_{Ri})^2$$

and from (10)

$$A_R \rightarrow \omega(1 - {V_{Ri}}^2/{\alpha_i}^2)^{1/2}/(4\rho_i {V_{Ri}}^3 D_i) \tag{17}$$

since $C_R \rightarrow U_R \rightarrow V_{Rj}$ with the subscript $j = 1$ for $\omega \rightarrow \infty$ and $j = n$ for $\omega \rightarrow 0$. This short-period expression is only valid for an all solid model; for oceanic models the limit is different and is not given here.

Expressions 12, 15, and 17 are identical with the limits given by *Harkrider* [1966], which were obtained by taking the short- and long-period limits of the residue evaluation of the solutions for buried sources.

Since the kinetic and potential energy integrals of (1) and (2) are equal for surface waves, we can write the spectral energy densities per unit propagation path as

$$E^R = \int_0^{2\pi} \omega^2 {I_0}^R \, |[w_0(r, \theta, h)]_R|^2 \, r \, d\theta \tag{18}$$

$$E^L = \int_0^{2\pi} \omega^2 {I_0}^L \, |\{V_0(r, \theta, h)\}_L|^2 \, r \, d\theta \tag{19}$$

Evaluating these expressions with the spectral solutions for buried sources in a multilayered medium [*Harkrider*, 1964; *Ben-Menahem and Harkrider*, 1964], we obtain at distances large in comparison with the wavelength

$${E_V}^R = \omega \langle L \rangle^2 C_R {A_R}^2 {I_0}^R [\dot{w}(h)/\dot{w}_0]^2 \tag{20}$$

$${E_V}^L \equiv 0 \tag{21}$$

for a vertical source at depth h and

$${E_H}^R = (\omega/2)\langle L \rangle^2 C_R {A_R}^2 {I_0}^R [\dot{u}^*(h)/\dot{w}_0]^2 \tag{22}$$

$${E_H}^L = (\omega/2)\langle L \rangle^2 C_L {A_L}^2 {I_0}^L [\dot{v}(h)/\dot{v}_0]^2 \tag{23}$$

for a horizontal source at the same depth with source strength $\langle L \rangle$.

Numerical Results

The numerical calculations presented in this paper are for two extreme models of the earth's mantle structure. The oceanic and shield models are given in Table 1 and Figure 1. These structures were derived by applying the universal

TABLE 2. Normalized Rayleigh and Love energy integrals in units of 10^5 ergs/cm^4 for the ocean structure.

RAYLEIGH

MODE 1,1		MODE 2,1		MODE 1,2	
PERIOD	ENERGY	PERIOD	ENERGY	PERIOD	ENERGY
350.	0.83660E 00	250.	0.16325E 02	110.	0.14421E 03
300.	0.81804E 00	225.	0.64546E 01	100.	0.49530E 02
250.	0.88346E 00	200.	0.69574E 01	90.	0.32500E 02
225.	0.96339E 00	175.	0.83638E 01	80.	0.22437E 02
200.	0.10855E 01	150.	0.10222E 02	70.	0.25950E 02
175.	0.12652E 01	140.	0.11232E 02	65.	0.33387E 02
150.	0.15293E 01	130.	0.12567E 02	60.	0.45168E 02
140.	0.16682E 01	120.	0.14359E 02	55.	0.60541E 02
130.	0.18320E 01	110.	0.16654E 02	50.	0.75620E 02
120.	0.20270E 01	100.	0.19313E 02	45.	0.85394E 02
110.	0.22610E 01	90.	0.21936E 02	40.	0.92823E 02
100.	0.25430E 01	80.	0.24208E 02	35.	0.11113E 03
90.	0.28900E 01	70.	0.27114E 02	30.	0.15659E 03
80.	0.33220E 01	65.	0.29916E 02	25.	0.26977E 03
70.	0.38762E 01	60.	0.34653E 02	20.	0.66251E 03
65.	0.42159E 01	55.	0.42459E 02	15.	0.34680E 04
60.	0.46101E 01	50.	0.55076E 02	10.	0.12420E 06
55.	0.50715E 01	45.	0.75520E 02		
50.	0.56159E 01	40.	0.10937E 03		
45.	0.62620E 01	35.	0.16760E 03		
40.	0.70303E 01	30.	0.27353E 03		
35.	0.79392E 01	25.	0.48540E 03		
30.	0.89970E 01	20.	0.10092E 04		
25.	0.10176E 02	15.	0.34319E 04		
20.	0.11292E 02	10.	0.49341E 05		
15.	0.12641E 02				
10.	0.37182E 02				

LOVE

MODE 0		MODE 1		MODE 2		MODE 3	
PERIOD	ENERGY	PERIOD	ENERGY	PERIOD	ENERGY	PERIOD	ENERGY
350.	0.46970E-00	200.	0.17491E 02	100.	0.42066E 02	65.	0.35565E 02
300.	0.56053E 00	175.	0.49721E 01	90.	0.13147E 02	60.	0.23841E 02
250.	0.71589E 00	150.	0.42305E 01	80.	0.12220E 02	55.	0.23117E 02
225.	0.83493E 00	140.	0.42787E 01	70.	0.14460E 02	50.	0.27401E 02
200.	0.99960E 00	130.	0.44409E 01	65.	0.15934E 02	45.	0.35680E 02
175.	0.12362E 01	120.	0.46938E 01	60.	0.17069E 02	40.	0.41048E 02
150.	0.15944E 01	110.	0.50199E 01	55.	0.17456E 02	35.	0.35297E 02
140.	0.17918E 01	100.	0.54117E 01	50.	0.17236E 02	30.	0.33503E 02
130.	0.20350E 01	90.	0.58904E 01	45.	0.17241E 02	25.	0.39507E 02
120.	0.23395E 01	80.	0.65398E 01	40.	0.18154E 02	20.	0.52621E 02
110.	0.27288E 01	70.	0.75425E 01	35.	0.20012E 02	15.	0.92548E 02
100.	0.32387E 01	65.	0.82664E 01	30.	0.22536E 02	10.	0.10480E 04
90.	0.39260E 01	60.	0.92062E 01	25.	0.25166E 02		
80.	0.48867E 01	55.	0.10432E 02	20.	0.26649E 02		
70.	0.62922E 01	50.	0.12040E 02	15.	0.27114E 02		
65.	0.72553E 01	45.	0.14172E 02	10.	0.29341E 04		
60.	0.84760E 01	40.	0.17039E 02				
55.	0.10058E 02	35.	0.20976E 02				
50.	0.12161E 02	30.	0.26519E 02				
45.	0.15050E 02	25.	0.34478E 02				
40.	0.19177E 02	20.	0.45034E 02				
35.	0.25378E 02	15.	0.41085E 02				
30.	0.35308E 02	10.	0.96181E 02				
25.	0.52538E 02						
20.	0.85064E 02						
15.	0.14116E 03						
10.	0.11985E 02						

dispersion theory of *Anderson* [1964] to the great-circle data of *Toksöz and Anderson* [1966]. Approximately 53 layers are used in each case to define the mantle structure.

For each model we provide in tables and/or figures the basic quantities necessary for calculating the surface wave energies for the first three Rayleigh and the first four Love modes. The effect of source depth is presented for the oceanic model, but tables for including the source depth can be found in *Harkrider* [1966] for a much wider range of depths for both models.

It is advisable at this point to mention some of the basic differences between the two structural models. The most pronounced difference

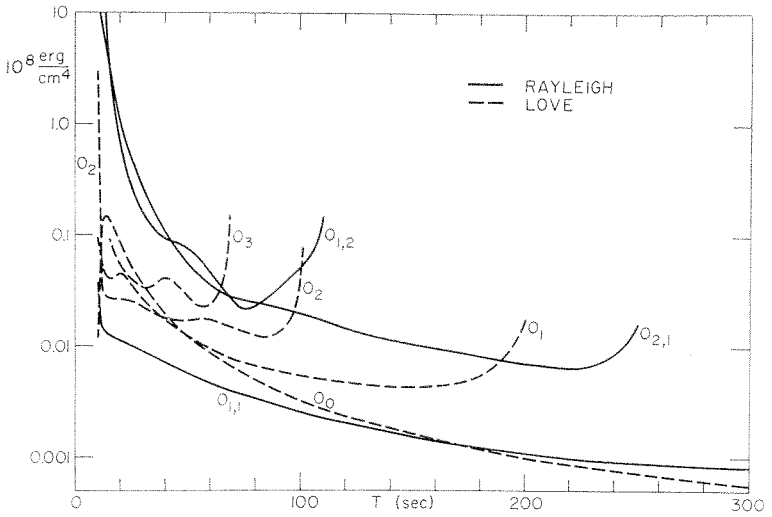

Fig. 2. Normalized Love and Rayleigh energy density integrals for the oceanic structure.

(Figure 1) occurs in the mantle low-velocity zone between 100 and 400 km. The oceanic model has a shallower and more pronounced low-velocity zone in addition to a thinner crustal wave guide. Thus, if any differences between models occur in the numerical results, we would expect them to be most apparent in the trapped modes, i.e., Love waves and the higher-mode Rayleigh waves. These are waves whose very existence depends on the presence of wave guides either at the surface or at depth, and they are thus more sensitive to the details of wave guides than the fundamental Rayleigh wave. The two pronounced upper mantle discontinuities at depths near 400 and 700 km are important features of recent conclusions regarding surface wave dispersion.

For the oceanic model, the sum of the normalized kinetic and potential energy density integrals are given in Table 2 and Figure 2. Since these two integrals are equal, the curves represent $2T^R$ and $2T^L$, given in (1) and (2). The same quantities are given for the shield model in Table 3 and Figure 3. From the limits (16) we see that the energy density integral for fundamental Rayleigh waves is inversely proportional to period at both the long and short periods. For the fundamental Love wave, the limits (11 and 13) require that the energy density integral approach a constant value at long periods and be inversely proportional to the square of the period at short periods.

From the figures we see that the long-period asymptotic behavior of the energy integrals is beyond the range of the tabulated results. In fact, on the basis of the figures alone, we might suspect that the quoted long-period trends of Love and Rayleigh waves had been interchanged. To verify the limits, we calculated the energy for very long periods, and the results agree with the theory.

At short periods the asymptotic trends of the Rayleigh and Love fundamental modes for the shield model can be seen in Figure 3. The relatively complicated behavior (Figure 2) at short periods is associated with the surface, crustal, and upper mantle wave guides. Complications occur at shorter periods for the oceanic model because of the thinner crust and shallower low-velocity zone.

As suggested earlier, the contrast between models is greatest in the trapped modes, especially the Love modes. Very little difference in the normalized energy densities of the fundamental Rayleigh waves occurs over the range of calculated periods.

Energy curves obtained by numerical integration can be found for additional earth models in *Wu* [1966].

To calculate the actual variation of energy with frequency and mode, we must operate on the normalized energies with the spectrum of surface displacements obtained from a given source.

TABLE 3. Normalized Rayleigh and Love energy integrals in units of 10^5 ergs/cm^4 for the shield structure.

RAYLEIGH

MODE 1,1		MODE 2,1		MODE 1,2	
PERIOD	ENERGY	PERIOD	ENERGY	PERIOD	ENERGY
350.	0.82251E 00	250.	0.10227E 02	110.	0.92987E 02
300.	0.84075E 00	225.	0.76901E 01	100.	0.49643E 02
250.	0.95077E 00	200.	0.87048E 01	90.	0.39277E 02
225.	0.10551E 01	175.	0.10385E 02	80.	0.29952E 02
200.	0.12047E 01	150.	0.12264E 02	70.	0.30086E 02
175.	0.14179E 01	140.	0.13251E 02	65.	0.35445E 02
150.	0.17265E 01	130.	0.14631E 02	60.	0.45002E 02
140.	0.18881E 01	120.	0.16646E 02	55.	0.59229E 02
130.	0.20785E 01	110.	0.19500E 02	50.	0.77096E 02
120.	0.23041E 01	100.	0.23265E 02	45.	0.94808E 02
110.	0.25733E 01	90.	0.27776E 02	40.	0.10864E 03
100.	0.28962E 01	80.	0.32732E 02	35.	0.12475E 03
90.	0.32855E 01	70.	0.38452E 02	30.	0.16470E 03
80.	0.37568E 01	65.	0.42406E 02	25.	0.27525E 03
70.	0.43286E 01	60.	0.48223E 02	20.	0.62521E 03
65.	0.46578E 01	55.	0.57510E 02	15.	0.20244E 04
60.	0.50181E 01	50.	0.73056E 02	10.	0.59404E 05
55.	0.54102E 01	45.	0.10031E 03		
50.	0.58320E 01	40.	0.15168E 03		
45.	0.62775E 01	35.	0.26026E 03		
40.	0.67344E 01	30.	0.53339E 03		
35.	0.71799E 01	25.	0.14271E 04		
30.	0.75815E 01	20.	0.57889E 04		
25.	0.79297E 01	15.	0.41643E 05		
20.	0.84183E 01	10.	0.76074E 02		
15.	0.98796E 01				
10.	0.14450E 02				

LOVE

MODE 0		MODE 1		MODE 2		MODE 3	
PERIOD	ENERGY	PERIOD	ENERGY	PERIOD	ENERGY	PERIOD	ENERGY
350.	0.50423E 00	200.	0.91849E 01	100.	0.18666E 02	70.	0.68627E 02
300.	0.60347E 00	175.	0.44218E 01	90.	0.11096E 02	65.	0.24230E 02
250.	0.76636E 00	150.	0.40184E 01	80.	0.10993E 02	60.	0.21196E 02
225.	0.88682E 00	140.	0.41098E 01	70.	0.13121E 02	55.	0.21948E 02
200.	0.10479E 01	130.	0.42951E 01	65.	0.14771E 02	50.	0.25579E 02
175.	0.12688E 01	120.	0.45574E 01	60.	0.16608E 02	45.	0.32761E 02
150.	0.15809E 01	110.	0.48806E 01	55.	0.18410E 02	40.	0.42492E 02
140.	0.17420E 01	100.	0.52507E 01	50.	0.20192E 02	35.	0.49513E 02
130.	0.19304E 01	90.	0.56674E 01	45.	0.22752E 02	30.	0.58877E 02
120.	0.21513E 01	80.	0.61762E 01	40.	0.28264E 02	25.	0.92299E 02
110.	0.24106E 01	70.	0.69340E 01	35.	0.41724E 02	20.	0.19191E 03
100.	0.27114E 01	65.	0.75198E 01	30.	0.78427E 02	15.	0.49828E 03
90.	0.30615E 01	60.	0.83746E 01	25.	0.20224E 03	10.	0.33544E 02
80.	0.34450E 01	55.	0.97237E 01	20.	0.79618E 03		
70.	0.38260E 01	50.	0.12099E 02	15.	0.57286E 04		
65.	0.39884E 01	45.	0.16961E 02	10.	0.37570E 04		
60.	0.41073E 01	40.	0.28948E 02				
55.	0.41597E 01	35.	0.65257E 02				
50.	0.41301E 01	30.	0.20271E 03				
45.	0.40342E 01	25.	0.88935E 03				
40.	0.39439E 01	20.	0.59845E 04				
35.	0.39808E 01	15.	0.71766E 05				
30.	0.42414E 01	10.	0.34283E 06				
25.	0.48462E 01						
20.	0.60783E 01						
15.	0.87437E 01						
10.	0.15755E 02						

To facilitate computation and comparison, we adopt as a standard spectrum that due to a surface point source. The spectral density of surface displacement due to a surface source is referred to as relative excitation in this paper. The relative excitations for Rayleigh and Love waves for the oceanic and shield models are given in Figures 4 and 5.

As with the normalized energy integrals, there is little difference between the two models in the relative excitation of fundamental Rayleigh waves from 300 to 20 seconds. The major differences occur in the trapped modes, especially the Love waves. The shift in amplitude toward the high frequencies in the oceanic relative to the shield model is presumably due to the thinner oceanic wave guide with the maximums for Love waves shifted approximately from 50

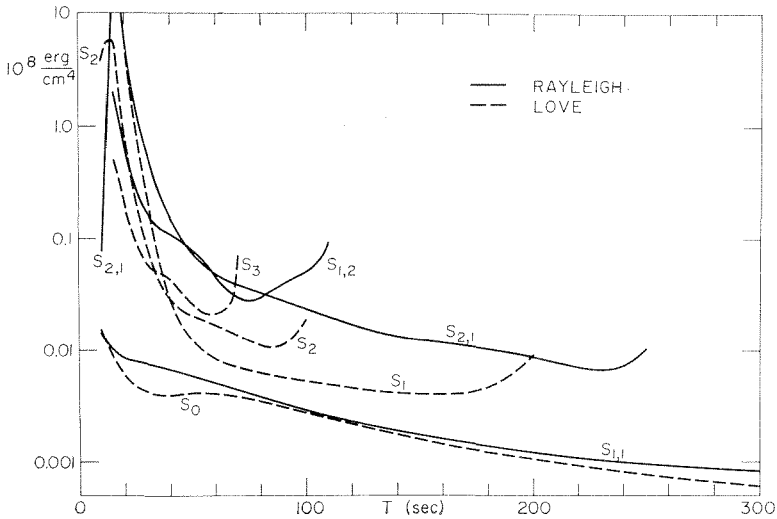

Fig. 3. Normalized Love and Rayleigh energy density integrals for the shield structure.

to 20 seconds. Note the increasing importance of the higher modes relative to the fundamental mode at intermediate periods.

Physically, these curves are the response of the medium to a surface source. Thus we would expect the amplitude of the trapped modes to become much smaller than the fundamental Rayleigh mode at low and high frequencies. This is reasonable because, at these limits, we are approaching half-space conditions for which Love waves and higher modes do not exist.

In Figure 6 we show the Rayleigh and Love wave energy densities per unit propagation path for surface sources at different orientations for oceanic and shield structures. In the figures, the single-subscripted dashed curves are Love modes, and the double-subscripted solid curves refer to Rayleigh modes. A vertical source, of course, does not generate Love waves.

In all cases the energy of the higher-mode Rayleigh waves is at least an order of magnitude less than that contained in the fundamental Rayleigh mode. This is in direct contrast to the normalized energies (Figures 2 and 3) where the opposite was true. Also, the energy in higher modes drops at both the long and short periods and, in all modes, at the long periods. The energies contained in the fundamental Love and Rayleigh modes are roughly comparable for a horizontal surface source, and the higher Love modes are much more energetic than the corresponding Rayleigh modes.

The importance of the short-period surface waves in any estimate of total surface wave energy is obvious from these figures. From (20), (22), and (23) we see that at long periods the fundamental Rayleigh mode is of the order of ω^2 and the fundamental Love mode is of the order ω^3. The greater energy in the trapped modes of the oceanic model relative to the shield model for a surface source reflects the relative nearness to the surface of the oceanic wave guides. As noted earlier for other spectral quantities, the energies for the fundamental Rayleigh mode are remarkably similar for the two models.

For a horizontal surface force, the energy density of the fundamental Rayleigh mode decreases by a factor of about 4. This can be seen quantitatively by comparing (20) with (22), since the square of surface ellipticity for fundamental Rayleigh waves is about 0.5 for a wide range of periods.

An assumption of equipartition of energy density between all surface wave modes is obviously not valid even for estimation purposes. On the other hand, there is to some degree an equipartition of energy density between the fundamental Rayleigh and fundamental Love modes for a horizontal surface source. This is true for both models. Also, as noted above, the higher Love modes contain more energy than the higher Rayleigh modes.

For certain frequencies the energy densities

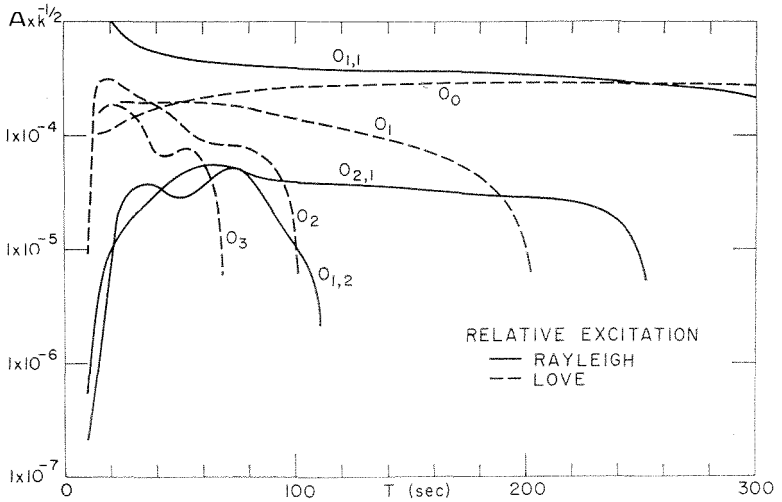

Fig. 4. Relative spectral excitation for the oceanic structure in units of $10^{-12.5}$ cm$^{3/2}$/dyne.

of higher-mode Rayleigh waves are approximately equal, and similarly for the higher-mode Love waves. Thus, in these frequency bands, a rough equipartition of energy density is obtained for the higher modes of Rayleigh and Love waves. For the oceanic model the equipartition includes the fundamental Love wave with its higher modes.

The effect of source depth on the first three Rayleigh modes for a vertical force in an oceanic model is illustrated in Figure 7. The figure at the top left is for the surface source given in Figure 6 and is used as a reference. At the top right we show the spectral energy density per unit propagation path for the fundamental mode for a surface focus and for three other source depths.

In general, increasing the depth decreases the amount of energy in the fundamental mode. However, a focus at 50 km, which is the top of the low-velocity zone, can generate Rayleigh waves with slightly more energy for certain frequencies than a surface source. The higher modes all have critical depths at which they are excited most efficiently and also periods at which they are not excited at all. For a given

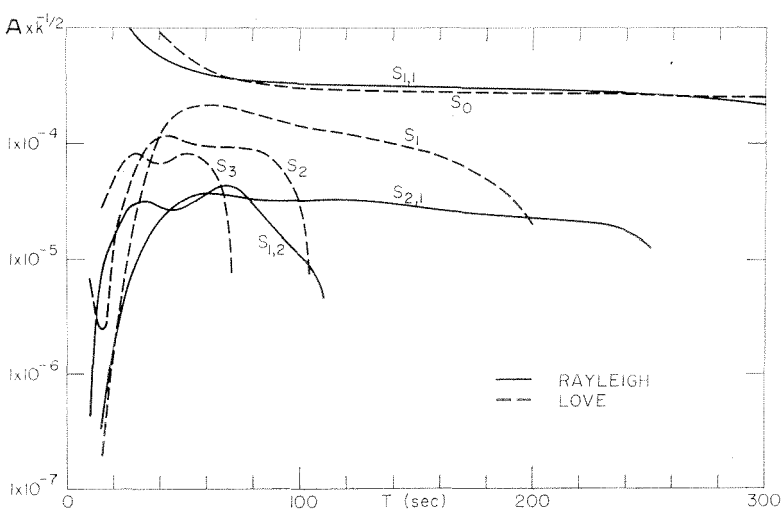

Fig. 5. Relative spectral excitation for the shield structure in units of $10^{-12.5}$ cm$^{3/2}$/dyne.

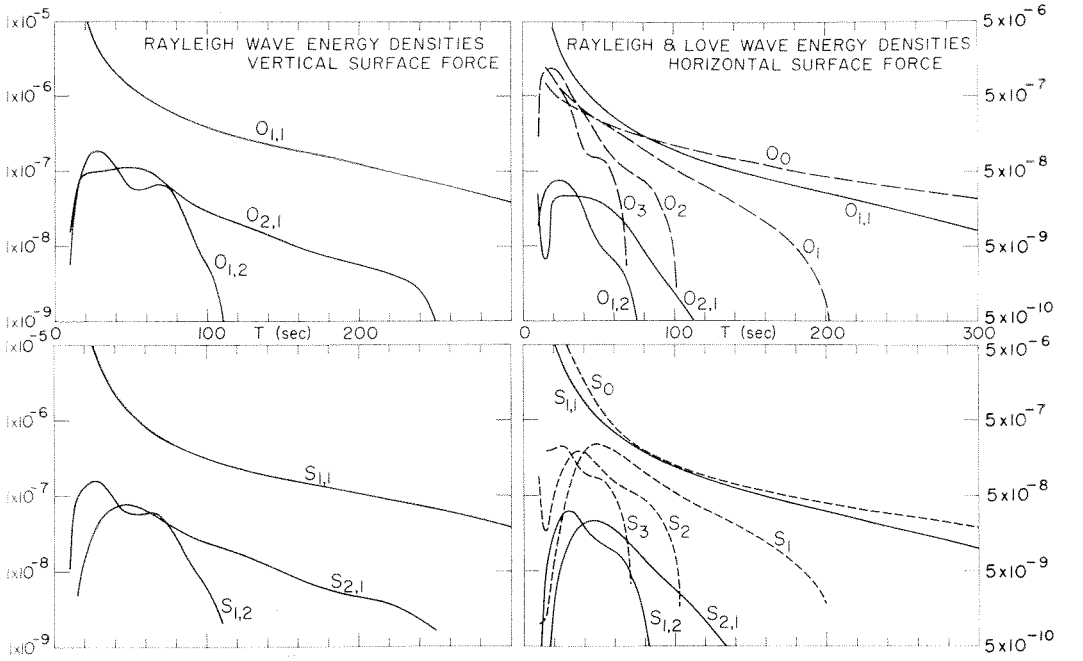

Fig. 6. Spectral energy densities per unit propagation path in units of 10^{15} ergs/km for a surface force of strength $\langle L \rangle = 10^{15}$ dynes sec.

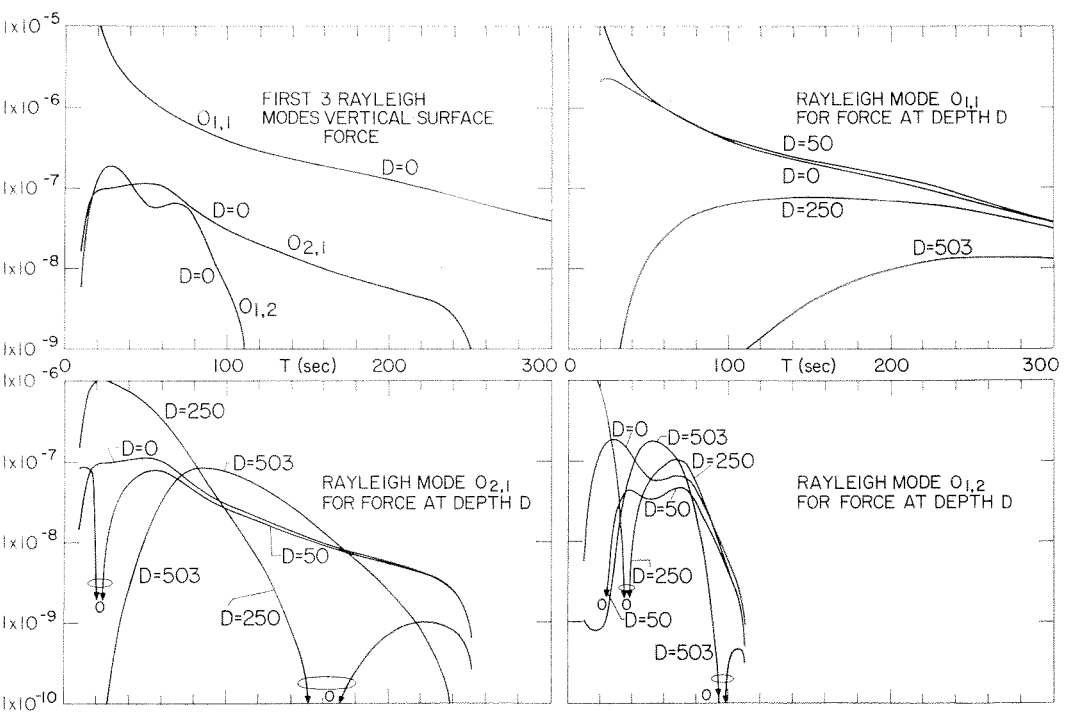

Fig. 7. Rayleigh wave spectrum energy densities per unit oceanic propagation path in units of 10^{15} ergs/km for buried vertical forces of strength $\langle L \rangle = 10^{15}$ dynes sec.

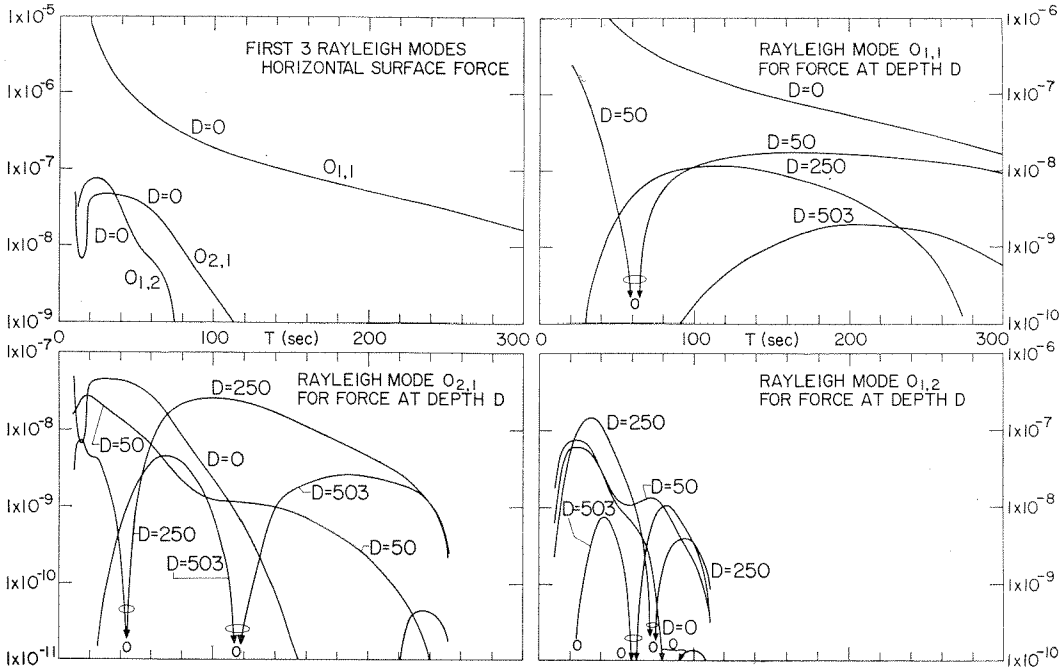

Fig. 8. Rayleigh wave spectrum energy densities per unit oceanic propagation path in units of 10^{15} ergs/km for buried horizontal forces of strength $\langle L \rangle = 2 \times 10^{15}$ dynes sec.

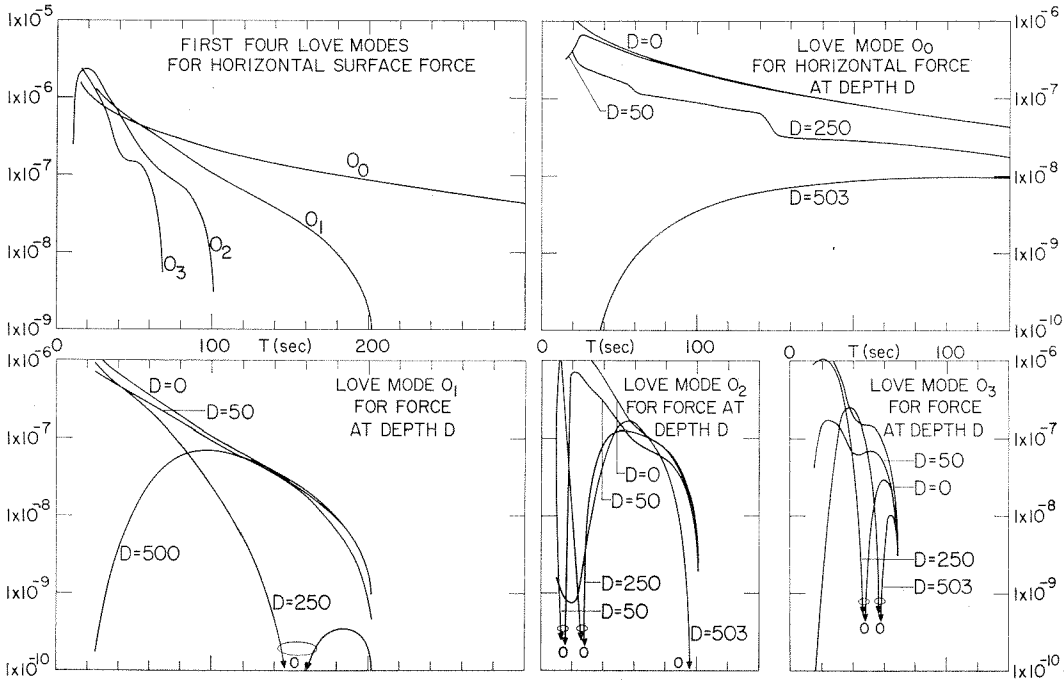

Fig. 9. Love wave spectrum energy densities per unit oceanic propagation path in units of 10^{15} ergs/km for buried horizontal forces of strength $\langle L \rangle = 2 \times 10^{15}$ dynes sec.

source orientation these zeros are diagnostic of source depth. Note the shift of the zeros with frequency for increasing source depth. The successively deeper sources have zeros at successively longer periods. A source at 250 km, which is in the low-velocity channel, is a very efficient generator of higher-mode waves.

Figure 8 shows the Rayleigh wave energy densities for horizontal forces at various depths. The important difference, for vertical and horizontal forces, is the shift in the location of the energy zeros. The zero locations for the two forces are governed by the nodes of horizontal displacements for horizontal forces and the nodes of the vertical displacements for vertical forces. The most efficient level for the generation of the fundamental mode for periods greater than 20 seconds is at the surface. A source in the channel generates less higher-mode energy than sources at other depths only for periods which involve a vertical displacement node in the channel. This again illustrates the channel wave characteristic of higher modes.

Even though a source in the channel is especially efficient in the generation of higher modes, it should be emphasized that this does not necessarily mean high surface amplitudes. Most of the energy is in the channel. On the other hand, small surface amplitudes of the higher modes do not mean low total energies. One cannot neglect the energy content of higher modes simply because they have low surface amplitudes.

The corresponding Love wave energy densities are displayed in Figure 9. As before, the holes in the energy spectrum of the higher modes are diagnostic of source depth.

Conclusions

The tables given in this paper make it possible to convert an observed surface wave amplitude at a given period to the total energy in the wave at that period, or to convert an observed amplitude spectrum over a certain frequency band to the total energy contained in that band. The figures given here and the tables in *Harkrider* [1966] make it possible to estimate the partitioning of energy among the various surface wave modes. The use of spectrums and nodal spectral ratios to recover source depth and orientation is discussed further in *Harkrider* [1966].

To estimate the energy in a frequency band from a seismic source, the data from several stations are needed to define the radiation pattern and source characteristics, which in turn are required for the surface integration. The experimental frequency band should be as wide as possible and, in particular, should include as much information as possible from the short-period arrivals. The curves presented here in conjunction with the asymptotic limits can be used in estimating the energy outside the measured band. The energy content of modes not directly analyzed can also be estimated if enough properties of the source are known. The experimental amplitude spectrums should, of course, be corrected for propagation effects such as spreading and attenuation.

Acknowledgment. This research was supported by the Advanced Research Projects Agency and was monitored by the Air Force Office of Scientific Research under contract AF-49(638)-1337.

References

Anderson, Don L., Universal dispersion tables, 1, Love waves across oceans and continents on a spherical earth, *Bull. Seismol. Soc. Am., 54,* 681–726, 1964.

Anderson, Don L., Latest information from seismic observations, in *The Earth's Mantle,* edited by T. F. Gaskell, Academic Press, London and New York, in press, 1966.

Anderson, Don L., and C. B. Archambeau, The anelasticity of the earth, *J. Geophys. Res., 69,* 2071–2084, 1964.

Anderson, Don L., A. Ben-Menahem, and C. B. Archambeau, Attenuation of seismic energy in the upper mantle, *J. Geophys. Res., 70,* 1441–1448, 1965.

Anderson, Don L., and M. N. Toksöz, Surface wave dispersion and structure of the upper mantle, in preparation, 1966.

Archambeau, C. B., and D. L. Anderson, Inversion of surface wave dispersion data, paper presented at IUGG 13th General Assembly, Berkeley, Calif., 1963.

Ben-Menahem, A., and D. G. Harkrider, Radiation patterns of seismic surface waves from buried dipolar point sources in a flat stratified earth, *J. Geophys. Res., 69,* 2605–2620, 1964.

Harkrider, D. G., Surface waves in multilayered elastic media, 1, Rayleigh and Love waves from buried sources in multilayered elastic half-space, *Bull. Seismol. Soc. Am., 54,* 627–679, 1964.

Harkrider, D. G., Surface waves in multilayered elastic media, 2, Higher mode spectra and spectral ratios from point forces in plane layered earth models, in preparation for the *Bull. Seismol. Soc. Am.,* 1966.

Haskell, N. A., The dispersion of surface waves in

multilayered media, *Bull. Seismol. Soc. Am., 43,* 17–34, 1953.

Kellis-Borok, V. I., and T. B. Yanovskaya, Dependence of the spectrum of surface waves on the depth of the focus within the earth's crust, *Bull. Acad. Sci. USSR, Geophys. Ser., English Transl.,* no. 11, 1532–1539, 1962.

Kovach, R. L., and Don L. Anderson, Higher mode surface waves and their bearing on the structure of the earth's mantle, *Bull. Seismol. Soc. Am., 54,* 161–182, 1964.

Jeffreys, H., The surface waves of earthquakes, *Monthly Notices Roy. Astron. Soc., Geophys. Suppl., 3,* 253–261, 1934.

Jeffreys, H., Small corrections in the theory of surface waves, *Geophys. J., 6,* 115–117, 1961.

Meissner, E., Elastiche oberflächen Querwellen, *Verhandl. Intern. Kongr. Tech. Mech., 2nd, Zurich,* 3–11, 1926.

Takeuchi, H., M. Saito, and N. Kobayashi, Study of shear velocity distribution in the upper mantle by mantle Rayleigh and Love waves, *J. Geophys. Res., 67,* 2831–2839, 1962.

Takeuchi, H., J. Dorman, and M. Saito, Partial derivatives of surface wave phase velocity with respect to physical parameter changes within the earth, *J. Geophys. Res., 69,* 3429–3441, 1964.

Toksöz, M. N., and Don L. Anderson, Phase velocities of long-period surface waves and structure of the upper mantle, 1, *J. Geophys. Res., 71,* 1649–1658, 1966.

Wu, Francis T., Energy of earthquakes, *Bull. Seismol. Soc. Am.,* in press, 1966.

(Manuscript received January 17, 1966.)